sustainability

MDPI

Article

Spatiotemporal Evolution and Drivers of Carbon Storage from a Sustainable Development Perspective: A Case Study of the Region along the Middle and Lower Yellow River, China

Shu An, Yifang Duan *, Dengshuai Chen and Xiaoman Wu

School of Geography and Environment, Liaocheng University, Liaocheng 252000, China; 2210140214@stu.lcu.edu.cn (S.A.); chendengshuai@lcu.edu.cn (D.C.); 2310140220@stu.lcu.edu.cn (X.W.)
* Correspondence: duanyifang@lcu.edu.cn

Abstract: Carbon storage (C-storage) is a critical indicator of ecosystem services, and it plays a vital role in maintaining ecological balance and driving sustainability. Its assessment provides essential insights for enhancing environmental protection, optimizing land use, and formulating policies that support long-term ecological and economic sustainability. Previous research on C-storage in the Yellow River Basin has mainly concentrated on the spatiotemporal fluctuations of C-storage and the investigation of natural influencing factors. However, research combining human activity factors to explore the influences on C-storage is limited. In this paper, based on the assessment of the spatiotemporal evolution of C-storage in the region along the Middle and Lower Yellow River (MLYR), the influences of anthropogenic and natural factors on C-storage were explored from the perspective of sustainable development. The findings reflected the relationship between socio-economic activities and the ecological environment from a sustainable development perspective, providing important scientific evidence for the formulation of sustainability policies in the region. We noticed the proportion of arable land was the highest, reaching 40%. The increase of construction land because of the fast urbanization mainly came from arable land and grassland. During the past 15 years, the cumulative loss of C-storage was 71.17×10^6 t. The high-value of C-storage was primarily situated in hilly areas, and the area of C-storage hotspots was shrinking. The aggregation effect of low-value C-storage was strengthening, while that of high-value C-storage was weakening. The dominant factors ($q > 0.5$) influencing the spatiotemporal variation of C-storage in the region along the Middle Yellow River (MYR) were temperature and precipitation, while the primary factor in the region along the Lower Yellow River (LYR) was temperature. Overall, meteorological factors were the main determinants across the entire study area. Additionally, compared to the MYR, anthropogenic factors had a smaller impact on the spatiotemporal evolution of C-storage in the LYR, but their influence has been increasing over time.

Keywords: carbon storage (C-storage); land use/cover changes; the Middle and Lower Yellow River (MLYR); sustainable development; sustainability; InVEST model; GeoDetector

Citation: An, S.; Duan, Y.; Chen, D.; Wu, X. Spatiotemporal Evolution and Drivers of Carbon Storage from a Sustainable Development Perspective: A Case Study of the Region along the Middle and Lower Yellow River, China. *Sustainability* **2024**, *16*, 6409. https://doi.org/10.3390/su16156409

Academic Editors: Baojie He, Siliang Yang, K. Venkatachalam, Amos Darko and Ali Cheshmehzangi

Received: 28 June 2024
Revised: 19 July 2024
Accepted: 24 July 2024
Published: 26 July 2024

1. Introduction

Rapid economic growth and urbanization has brought a rapid expansion of construction land, led to the dramatic alteration in the composition of land use, and has increased the emission of carbon dioxide and other greenhouse gases. Worldwide carbon emission is projected to rise from 2010 to 30% by 2030 [1–3]. As a result, improving C-storage and reducing carbon emissions have emerged as critical issues in today's society to help mitigate global warming and advance sustainable development [4,5].

Land use/cover change (LUCC) is among the crucial factors influencing alterations in plant and soil C-storage. This, still further, affects the overall C-storage of the whole region, thereby altering ecosystem structure and function and the ecosystem carbon cycling process [6]. Early land-use research was primarily supported by the spatial technologies

of systems for geographic information and remote sensing [7], which allowed researchers both domestically and internationally to conduct land-use-related surveys, evaluate land resources [8], and plan and manage land use [9]. As research has advanced, academics have mostly concentrated on examining the drivers that have shaped land-use patterns at various sizes [10]. Changes in land usage and C-storage are among the most closely coupled and interactive components in natural development. Enhancing the ability to sequester carbon in regional ecosystems can be achieved through the land use structure's optimization [11]. A growing body of academics has devoted themselves to assessing historical land-use changes and forecasting future changes, as well as exploring the connection amidst changes in land utilization and modifications in C-storage. This holds significant implications for implementing rational land planning and management policies at the regional level and promoting socio-economic development in a healthy manner [12,13].

The C-storage of a terrestrial ecosystem serves as a crucial metric for assessing the functionality of regional ecosystem services. Accurate quantification of C-storage at various scales holds significant scientific importance in formulating strategies to mitigate global warming. In this regard, scholars from both domestic and international arenas have embarked upon exploring diverse methodologies for C-storage estimation. A plot-based inventory method was utilized in determining the quantity of C-storage of forest [14], while field measurement techniques of soil carbon density was used to quantify the soil organic carbon content [15]. These methods, which are based on field measurements, are more accurate on a small scale, but have the disadvantage of a long data-collection period and a heavy workload, making it difficult to apply them on a large scale. With the development of remote sensing technology, the FORCCHN model has been used to quantify ecosystem C-storage by simulating carbon cycling processes in forest ecosystems [16]. However, it has high computational complexity and requires large amounts of data. Additionally, the DNDC model was widely used to simulate soil carbon and could model the impact of different management practices and climate change on C-storage [17]. Despite this, it requires extensive input data and complex parameter settings, and its regional applicability is limited. Similarly, the BEPS model also has high computational complexity and is primarily applied to northern ecosystems, limiting its use in other regions [18]. In contrast, the InVEST model is favored for its faster operation, lower data requirements, high applicability, and well-visualized results, making it widely used in ecosystem C-storage estimation [19]. The InVEST model has been widely applied to ecosystem C-storage studies across various scales, including provinces [11], cities [20], counties [21], and urban agglomerations [22], as well as different landforms such as wetlands [23], coastal areas [24], and plateaus [25].

In China, the Yellow River Basin holds considerable significance as it serves as a vital ecological security barrier and plays a pivotal role in population activities and economic development. It is a key component of China's overall socialist modernization efforts. Currently, numerous scholars have been conducting research on C-storage in the Yellow River Basin. Initially, remote sensing and GIS technology were used to assess the distribution and change of C-storage in urban trees [26]. The current and future LULC change processes and their impact on C-storage in the Yellow River Basin were explored [27]. Moreover, the influence of land use change on blue carbon accumulation along the Yellow River Delta coast was studied [5,28]. In summary, previous research primarily focused on single-factor land use studies regarding C-storage in the Yellow River Basin, lacking an in-depth exploration of multiple influencing factors. Specifically, there is a lack of previous research on the impact of the sustainable interaction between human activities and the natural environment on C-storage. Instead, this paper selected influencing factors based on both the natural environment and human activities and explored C-storage drivers from a sustainable development perspective.

Over 40% of the entire region's area along the MLYR is covered by forest and grassland, and the region is crucial for carbon sequestration in China's land-based ecology. Moreover, the region along the MLYR is characterized by frequent human activities, active socio-economic development, and rapid urbanization. Among them, the region along the MYR is

an important implementation area for the policy of converting farmland back into forests, while the region along the LYR has experienced rapid socio-economic development and urban expansion, and the land-use types across the region have changed drastically due to human intervention. Therefore, human activity's intervention in the C-storage within the area along the MLYR cannot be overlooked.

In this paper, the C-storage in the region along the MLYR was first measured using land use and corrected carbon density data by the InVEST model. Subsequently, GeoDetector was applied to detect and analyze the factors influencing C-storage in the region along the MYR and LYR, respectively. In the selection of driving factors, not only natural factors but also those reflecting the interaction between human activities and the natural environment were considered, with the aim of helping the region achieve sustainable development goals by harmonizing economic development with environmental protection.

2. Study Area and Data Sources

2.1. Overview of the Study Area

The study region (107°18′~119°18′ E, 33°36′~39°42′ N) includes 24 prefectures in Shandong, Henan, Shanxi, and Shaanxi province, with a total area of about 3.016×10^5 km^2 (Figure 1). The principal watercourse of the Yellow River runs through the study area, with the Loess Plateau in the west and the North China Plain in the east. The topography of the research region decreases gradually spanning from the northwest towards the southeast, with a mean elevation of 1500~3000 m in the northwest, 500~1000 m in the southwest, and about 50~1000 m in the east. The region experiences an average yearly temperature recorded at 10.03 °C and an average yearly rainfall of 481.4 mm. The region along the MLYR has nurtured different topographical features and rich human resources, and the resident population reached 111.5×10^6 in 2021.

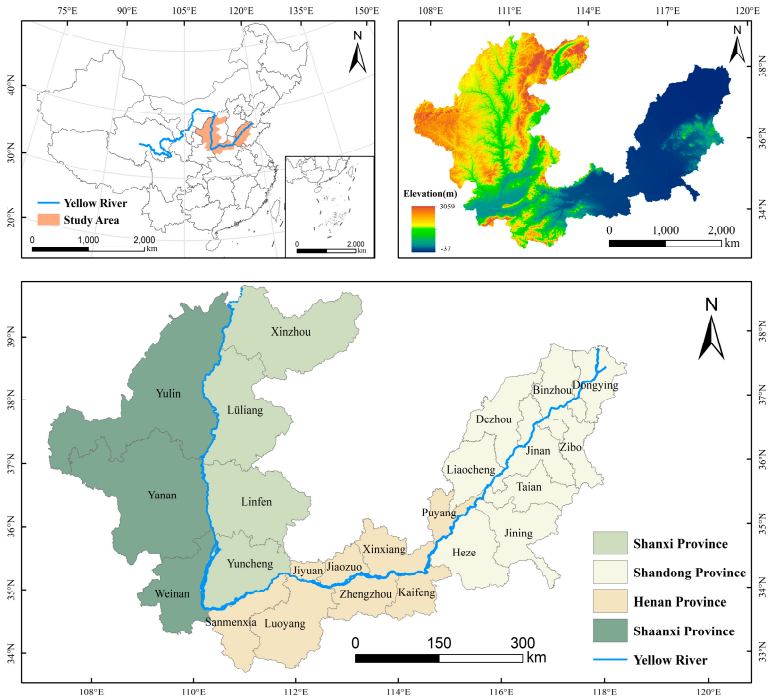

Figure 1. The geographic location and altitude of the study area.

2.2. Data Sources and Processing

(1) Land use/cover data were derived from 30 m resolution land cover products obtained using Landsat satellite imagery on Google Earth Engine by Prof. Huang's research team at the School of Remote Sensing and Information Engineering, Wuhan University [29]. In this study, the land use/cover data for four periods were clipped to the study area. Subsequently, the data were reclassified into six categories based on Liu Jiyuan's land

use classification method [30]: arable land (AL), forest land (FL), grassland (GL), water (WL), construction land (CL), and unused land (UL). This reclassified data serves as the basis for analyzing land-use changes and estimating C-storage. Additionally, we calculated the composite land-use extent index data based on the processed land-use data [31]. (2) Digital Elevation Model (DEM) data were obtained from the Resource and Environment Science Data Center, and slope data were derived from the DEM. (3) Temperature and precipitation data were obtained from the National Tibetan Plateau Data Center [32,33]. Due to the interannual variability of these meteorological factors, the 20-year average temperature and precipitation data (20002020) were calculated and used for analyzing the factors influencing C-storage. (4) Fractional vegetation cover data were obtained from the National Tibetan Plateau Data Center [34]. (5) Human footprint data depict the impact of human activities on the Earth's surface, sourced from the annual dataset provided by the Urban Environmental Monitoring and Modeling (UEMM) team at the College of Land Science and Technology, China Agricultural University [35]. The values range from 0 to 50, with higher values indicating more frequent human activities. (6) Carbon density data were primarily referenced from the National Ecosystem Science Data Center and regions similar or adjacent to the study area [27,36], and they were corrected using a carbon density correction model.

In this study, the raster data were projected into a unified coordinate system (WGS_1984_UTM_Zone_49N) and clipped to the study area's extent using ArcGIS, ensuring consistency in projection and data coverage. Additionally, since a fishnet was created based on the study area to extract point data for various factors, the spatial resolution of different data was not unified to ensure data accuracy. The data types and sources are shown in the following table (Table 1).

Table 1. Data types and sources.

Data Types		Years	Sources
Vector	Population	2021	<<Shandong Statistical Yearbook>>/<<Henan Statistical Yearbook>> /<<Shanxi Statistical Yearbook>>/<<Shaanxi Statistical Yearbook>>
	Administrative Divisions	2015	National Catalogue Service for Geographic Information https://www.webmap.cn/ (accessed on 6 January 2023)
	River		
Land Use	LULC (30 m)	2005/2010 /2015/2020	<<The 30 m annual land cover datasets and its dynamics in China from 1985 to 2022>> https://doi.org/10.5281/zenodo.8176941
Terrain	DEM (90 m)	-	Resource and Environment Science and Data Center https://www.resdc.cn/ (accessed on 10 January 2023)
	Slope (90 m)		
Vegetation	Composite Land-use Extent Index (30 m)	2005/2010 /2015/2020	Calculated from land-use data
	Fractional Vegetation Cover (250 m)		<<China regional 250 m fractional vegetation cover data set (2000–2023)>> https://doi.org/10.11888/Terre.tpdc.300330
Meteorology	Temperature (1 km)	2000–2020	<<1-km monthly mean temperature dataset for china (1901–2022)>> https://doi.org/10.11888/Meteoro.tpdc.270961
	Precipitation (1 km)		<<1-km monthly precipitation dataset for China (1901–2022)>> https://doi.org/10.5281/zenodo.3185722
Human Activities	Human Footprint (30 m)	2005/2010 /2015/2020	<<A global record of annual terrestrial Human Footprint dataset from 2000 to 2018>> https://doi.org/10.1038/s41597-022-01284-8
Carbon Density	Original carbon density	-	National Ecosystem Science Data Center http://www.cnern.org.cn (accessed on 8 January 2023) <<Spatial and temporal variation of carbon stocks in the Yellow River basin based on InVEST and CA-Markov models>> http://doi.org/10.13930/j.cnki.cjea.200746 <<Effects of land use/cover change on carbon storage between 2000 and 2040 in the Yellow River Basin, China>> https://doi.org/10.1016/j.ecolind.2023.110345

3. Methodology

Based on the matrix of land utilization transfer, these time-space variations of land use were analyzed from 2005 to 2020. Then, combined with adjusted carbon density data, the C-storage was calculated with the InVEST model across different time periods. Finally, the C-storage drivers in the MYR and LYR were probed with the GeoDetector model, respectively, to find the heterogeneity and assist in the formulation of carbon-sequestration schemes based on local conditions (Figure 2).

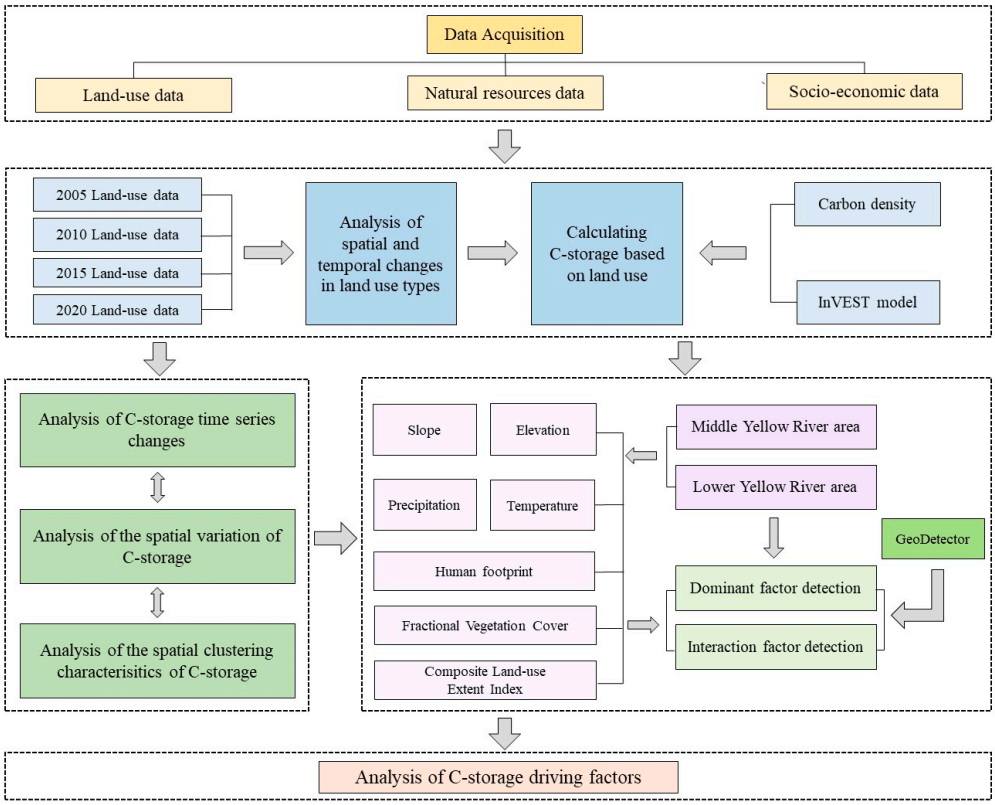

Figure 2. The technology roadmap of this investigation.

3.1. InVEST Model

InVEST is applied extensively to quantify ecosystem service value under different land-use scenarios, and its Carbon module is used extensively in the calculation and analysis of C-storage. Within this article, C-storage in the region along the MLYR was calculated with the InVEST model. Then, an analysis was conducted on the characteristics pertaining to the allocation of C-storage, and C-storage was categorized into four primary carbon reservoirs: aboveground, belowground, soil, and dead organic carbon. Data on land utilization and carbon density dictate the amount that each carbon pool holds. Each carbon pool's capacity for C-storage is ultimately combined to get the total C-storage (C_t, t ha^{-1}) over the research region. The calculating formula is as follows:

$$C_t = C_a + C_b + C_s + C_d \quad (1)$$

where C_t indicates the overall C-storage; C_a indicates C-storage above the surface; C_b indicates subterranean biological carbon sequestration; C_s indicates storage of organic carbon in the soil; and C_d indicates C-storage in deceased organic matter.

Since the carbon density data in this study reference results from different regions, and carbon density values vary due to differences in soil types, vegetation, and climate conditions, we need to correct the original carbon density values based on the long-term average temperature and precipitation data for the region along the MLYR and China.

Based on meteorological data [32,33], we calculated the multi-year average temperature and precipitation for the region along the MLYR to be 10.03 °C and 481.40 mm, respectively, and for China to be 8.93 °C and 672.00 mm, respectively. We used the formulas from Alam [37] (Equations (2) and (3)) to adjust for precipitation and the formula from Giardina and Chen [38,39] (Equation (4)) to adjust for average annual temperature and biomass carbon density. The specific formulas are as follows:

$$C_{Ax} = 3.398 \times P + 1996.1\left(R^2 = 0.11\right) \quad (2)$$

$$C_{Bx} = 6.7981e^{0.00541P}\left(R^2 = 0.70\right) \quad (3)$$

$$C_{By} = 28 \times T + 398\left(R^2 = 0.47, P < 0.01\right) \quad (4)$$

where C_{Ax} is the soil carbon density (kg m^{-2}) obtained from annual precipitation; C_{Bx} and C_{By} are the biomass carbon density (kg m^{-2}) obtained from annual precipitation and mean annual temperature, respectively; P is the mean annual precipitation; and T is the mean annual temperature (°C). The average annual temperature and annual precipitation of the region along the MLYR and China, respectively, are substituted into the above equation, and the ratio of the two is the correction factor. The product of the carbon density data and the correction factor is the carbon density data of this study area.

$$K_{Bx} = \frac{C'_{Bx}}{C''_{Bx}} \quad (5)$$

$$K_{By} = \frac{C'_{By}}{C''_{By}} \quad (6)$$

$$K_B = K_{By} \times K_{Bx} \quad (7)$$

$$K_A = \frac{C'_{Ax}}{C''_{Ax}} \quad (8)$$

where K_{Bx} and K_{By} are the correction coefficients of precipitation factor and temperature factor for biomass carbon density; C'_{Bx} and C''_{Bx} are the biomass carbon density data obtained from annual precipitation in the region along the MLYR and China, respectively; C'_{By} and C''_{By} are the biomass carbon density data obtained from the annual mean temperature in the region along the MLYR and China, respectively; C'_{Ax} and C''_{Ax} are the soil carbon density data obtained from annual precipitation in the region along the MLYR and China, respectively; and K_B and K_A are the biomass carbon density correction coefficients and soil carbon density correction coefficients, respectively. The corrected carbon density data in the region along the MLYR are shown in the following table (Table 2).

Table 2. Carbon density of each land-use type used in the InVEST model (t ha^{-1}).

Land-Use Type	C_a	C_b	C_s	C_d
Arable land (AL)	6.6	31.4	97.2	3.8
Forest land (FL)	16.5	45	142.4	5.5
Grassland (GL)	13.7	33.6	89.6	2.8
Water (WL)	0.1	0	0	0
Construction land (CL)	1	10.7	0	0
Unused land (UL)	0.5	0	19.4	0

3.2. GeoDetector

GeoDetector serves as a statistical method for measuring the diversity in geographical layering [40]. GeoDetector can combine quantitative data with qualitative data, and this

approach also clarifies the effects of a pair of explanatory factors interacting with each other on a particular target variable [41].

In this study, we selected natural factors from terrain (Elevation X1, Slope X2), meteorology (Temperature X3, Precipitation X4), and vegetation (Fractional Vegetation Cover X5). In addition, based on the sustainable development perspective, we also selected anthropogenic factors (Composite Land-use Extent Index X6, Human Footprint X7). The study area features significant variations in elevation and slope, which directly affect regional vegetation types and land-use types, so elevation and slope were chosen as topographic factors. Temperature and precipitation are key determinants of soil moisture and vegetation growth, with considerable differences in meteorological conditions between the region along the MYR and LYR, so they were chosen as meteorological factors. Instead of the Normalized Difference Vegetation Index (NDVI), we selected Fractional Vegetation Cover (FVC) as the vegetation factor, which more accurately reflects actual vegetation conditions. Given that the region along the MLYR is densely populated and economically active, we selected the Composite Land-use Extent Index (CLEI) to reflect the impact of various human activities on land types and ecosystems and the human footprint to quantify the overall impact of human activities on the natural environment. Based on this, we explored the main driving factors and interaction between factors of C-storage within the region along the MYR and LYR with GeoDetector, respectively.

3.2.1. Factor Detection

In order to reveal the degree to which the independent variable (X) is influential on the dependent variable (Y), its explanatory power is commonly expressed statistically as the *q*-value, which varies between 0 and 1. An elevated *q*-value signifies a more robust explanatory capacity of factor X for the dependent variable Y, which is computed as follows [42]:

$$q = 1 - \frac{\sum_{Z=1}^{G} F_Z \beta_Z^2}{F\beta^2} = 1 - \frac{BBW}{BBT} \tag{9}$$

$$BBW = \sum_{Z=1}^{G} F_Z \beta_Z^2 \tag{10}$$

$$BBT = F\beta^2 \tag{11}$$

where Z = 1, ..., G is the univariate stratification of Y or the factor X; F_Z represents the number of cells in layer Z, whereas F represents the number of cells in the overall area; β_Z^2 and β^2 represent the fluctuations in the Y values within layer Z and the entire area, in that order; and BBW and BBT represent the within-layer variation and the total fluctuation across the entire region, respectively.

3.2.2. Interaction Detection

The current research used the interaction detection approach to evaluate if the interaction between two independent variables, X1 and X2, amplifies or reduces the explanatory capacity of the dependent variable, Y. The interactions between two factors were classified by comparing the q-values of the single factors q(X1) and q(X2). Interaction types of factors are available on the GeoDetector software tool description website: http://www.geodetector.cn/ (accessed on 25 April 2023) [43].

4. Results

4.1. Temporal and Spatial Evolution of Land Use

AL, GL, and FL were the main types of land usage in the region along the MLYR and more than 80% of the entire surface area. The AL had the biggest share, followed by GL and FL. WL and UL made up less than 5% of the overall land (Table 3). AL continually decreased, featuring a yearly average alteration of 0.80 $\times$ 10^5 ha a^{-1} and CL, FL, and UL continually

increased, with CL seeing the biggest average annual change of 0.65 × 10^5 ha a^{-1}, while GL and WL were largely stable. Considering the aspect of view of geographical dispersion, the distribution of AL was mostly concentrated in the Guanzhong Plain region in the west and the North China Plain region in the central-east, GL in the western Loess Plateau region, and FL in the south and east of the Loess Plateau and the Qinling Mountains. In addition, a small amount of FL was also distributed in the central hilly areas of Shandong Province (Figure 3).

Table 3. Area changes for different land-use types from 2005 to 2020.

Land-Use Type	2005		2010		2015		2020		Area Change (10^5 ha)
	Area (10^5 ha)	Proportion	Area (10^5 ha)	Proportion	Area (10^5 ha)	Proportion	Area (10^5 ha)	Proportion	
Arable land (AL)	152.69	48.60%	147.84	47.06%	143.31	45.62%	140.63	44.77%	−12.06
Forest land (FL)	49.19	15.66%	50.50	16.08%	52.48	16.71%	54.13	17.23%	4.94
Grassland (GL)	81.81	26.04%	82.93	26.40%	82.78	26.35%	80.72	25.70%	−1.09
Water (WL)	3.68	1.17%	4.11	1.31%	4.27	1.36%	4.78	1.52%	1.10
Construction land (CL)	23.68	7.54%	26.78	8.53%	30.09	9.58%	33.49	10.66%	9.81
Unused land (UL)	3.10	0.99%	1.97	0.63%	1.21	0.38%	0.39	0.12%	2.71

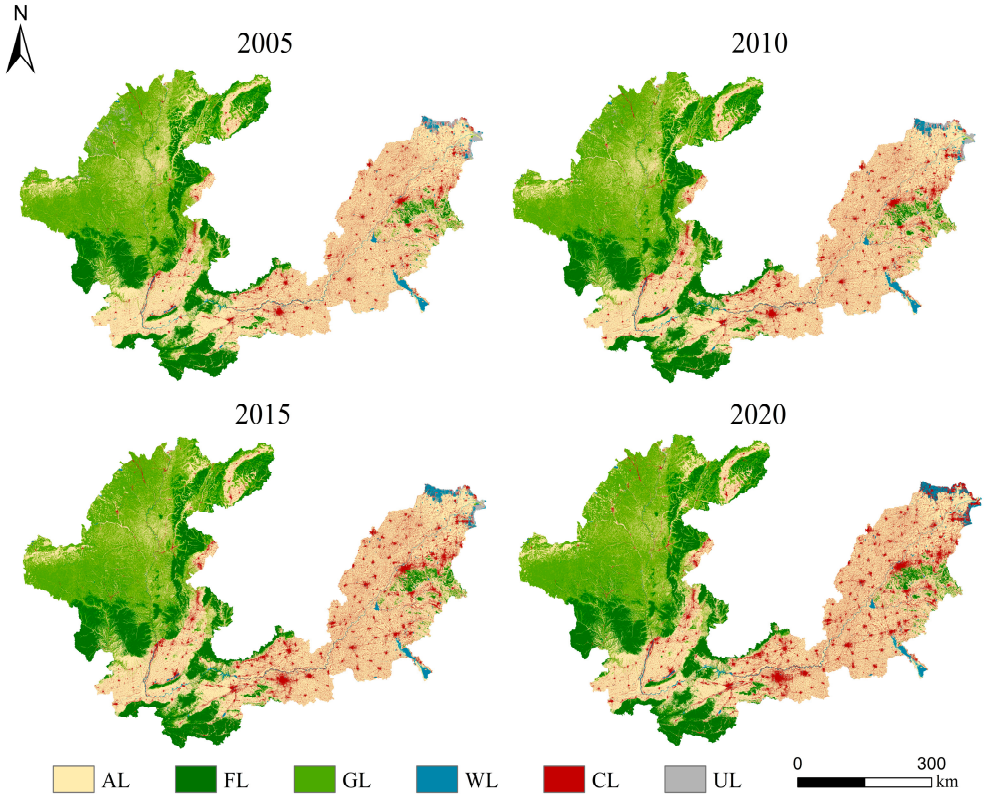

Figure 3. Spatial distribution of land-use types in the region along the MLYR from 2005 to 2020.

There was an obvious spatial heterogeneity of land-use change in the region along the MLYR. In the past 15 years, there were main transfers of four land-use types, "AL—CL", "AL—GL", "GL—AL", and "GL—FL" (Figure 4). Among others, the predominant conversion was observed between AL and CL, with the subsequent conversion occurring between AL and GL. Specifically, the largest decrease in AL (4.85 × 10^5 ha) occurred from 2005 to 2010 due to the enactment of the "Grain for Green" strategy; a significant portion of the AL had been transformed into areas for CL and GL. The largest increase in CL (9.81 × 10^5 ha) occurred from 2005 to 2020 under the influence of urbanization. The conversion of AL, resulting in the reduction of CL in the central and eastern regions of the country, and the extension of CL in the western region, were reflected in space. In addition, GL exhibited an upward trajectory from 2005 to 2010 followed by a downward trend from

2010 to 2020, and mainly shifted to AL and FL. As a whole, the expansion of CL occurred more quickly than the expansion of FL and WL, which adversely affected the growth of regional C-storage.

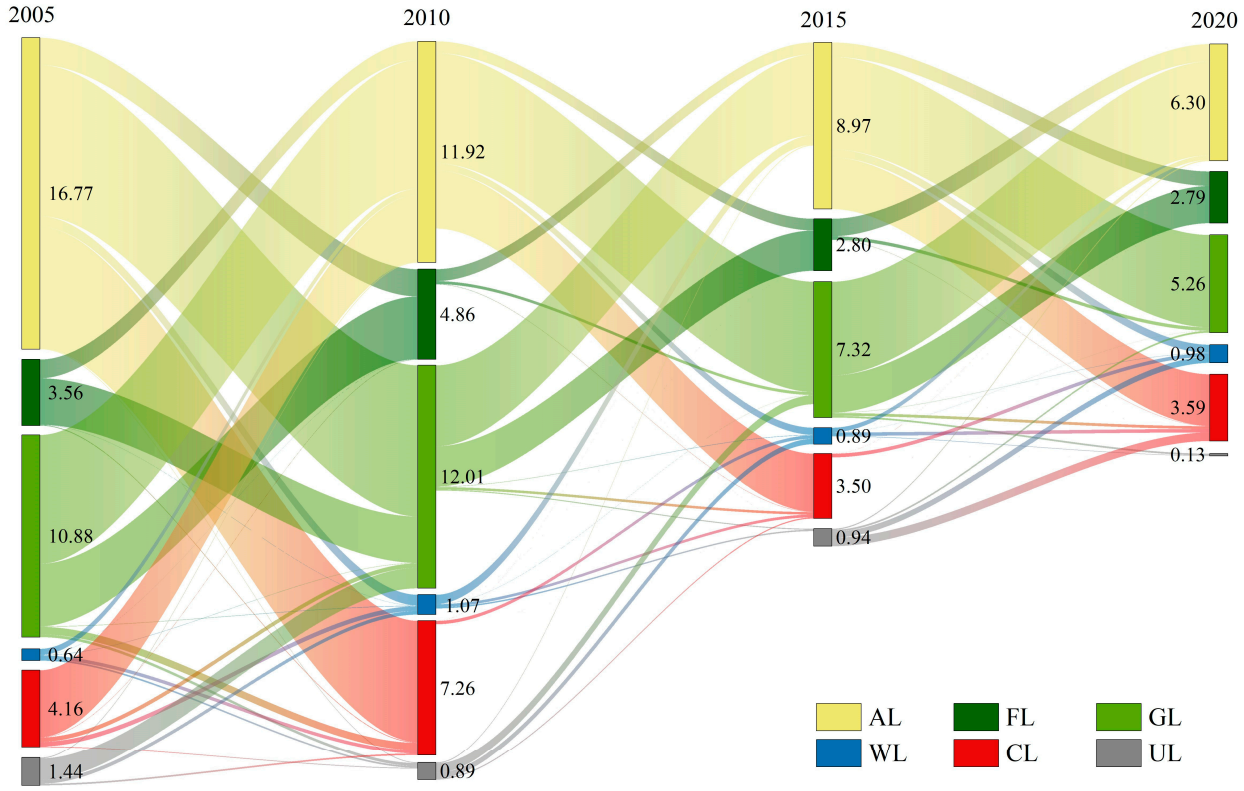

Figure 4. Transfer trajectory map of land-use type in the region along the MLYR from 2005 to 2020 (10^5 ha).

4.2. Temporal and Spatial Evolution of C-Storage

4.2.1. Temporal Variation Characteristics of C-Storage

From 2005 to 2020, the C-storage in the region along the MLYR showed a general trend of continuous decrease, but the decrease was not significant. During the 15 years, the cumulative loss of C-storage was 71.17 × 10^6 t, exhibiting a mean yearly decline rate of 0.14%. Of these, total C-storage was reduced by 28.41 × 10^6 t from 2015 to 2020, which is the largest stage of C-storage loss (Table 4). From a municipal scale, as the execution of this policy "returning farmland to forest" and "Three Norths", carbon density in Yulin, Xinzhou, Linfen, and Yan'an demonstrated a progressive incline from 2005 to 2020. However, the carbon density of the remaining prefecture-level cities showed a decreasing trend (Table 5).

Table 4. Changes in C-storage of ecosystems in the region along the MLYR from 2005 to 2020 (10^6 t).

Year	2005	2010	2015	2020	2005–2010	2010–2015	2015–2020	2005–2020
					Amount/Rate of Change	Amount/Rate of Change	Amount/Rate of Change	Amount/Rate of Change
Total	4221.13	4199.00	4178.47	4150.06	−22.22	−20.53	−28.41	−71.17
					0.53%	0.49%	1%	1.69%

Table 5. Carbon intensity of 24 prefecture-level cities from 2005 to 2020 (t ha^{-1}).

City	2005	2010	2015	2020	City	2005	2010	2015	2020
Dongying	8.591	8.297	7.893	7.200	Xinxiang	10.664	10.503	10.300	10.105
Jining	9.408	9.103	9.081	8.926	Zibo	10.838	10.550	10.427	10.333
Binzhou	9.508	9.231	8.981	8.648	Yulin	11.450	11.681	11.784	11.773
Puyang	9.744	9.588	9.348	9.087	Yuncheng	12.184	12.037	11.938	11.841
Dezhou	9.762	9.638	9.442	9.334	Weinan	12.195	12.103	11.991	11.858
Liaocheng	9.905	9.739	9.529	9.340	Jiyuan	12.756	12.798	12.409	12.450
Zhengzhou	10.101	9.848	9.392	8.923	Xinzhou	12.956	12.958	12.977	13.050
Heze	10.124	9.917	9.670	9.442	Linfen	13.197	13.199	13.249	13.278
Taian	10.245	10.069	9.959	9.793	Lvliang	13.264	13.226	13.239	13.229
Kaifeng	10.279	10.126	9.913	9.662	Luoyang	13.771	13.670	13.563	13.593
Jinan	10.531	10.252	10.118	9.992	Yanan	14.005	14.054	14.199	14.277
Jiaozuo	10.622	10.425	10.081	9.867	Sanmenxia	14.562	14.485	14.478	14.553

4.2.2. Spatial Variation Characteristics of C-Storage

This spatial distribution of C-storage had a relatively significant spatial heterogeneity in the region along the MLYR. As a whole, the C-storage showed a geographical distribution characterized by elevated levels in the western regions and diminished levels in the eastern regions, with increased levels in mountains and decreased levels in plains (Figure 5). The eastern and southern Loess Plateau and Qinling Mountains regions exhibited a significant concentration of C-storage's high value, and the hilly areas of Shandong Province also had a relatively high C-storage value. The primary factor contributing to the high C-storage in the above region was the land-use types, which consists mostly of FL with dense plant cover, and where the carbon density can be as high as 18 t ha^{-1}. Areas exhibiting minimal C-storage capacity were predominantly located in the central Guanzhong Plain and the eastern North China Plain region, where land-use types were mainly AL and CL, with large disturbances from human activities and low carbon sink capacity.

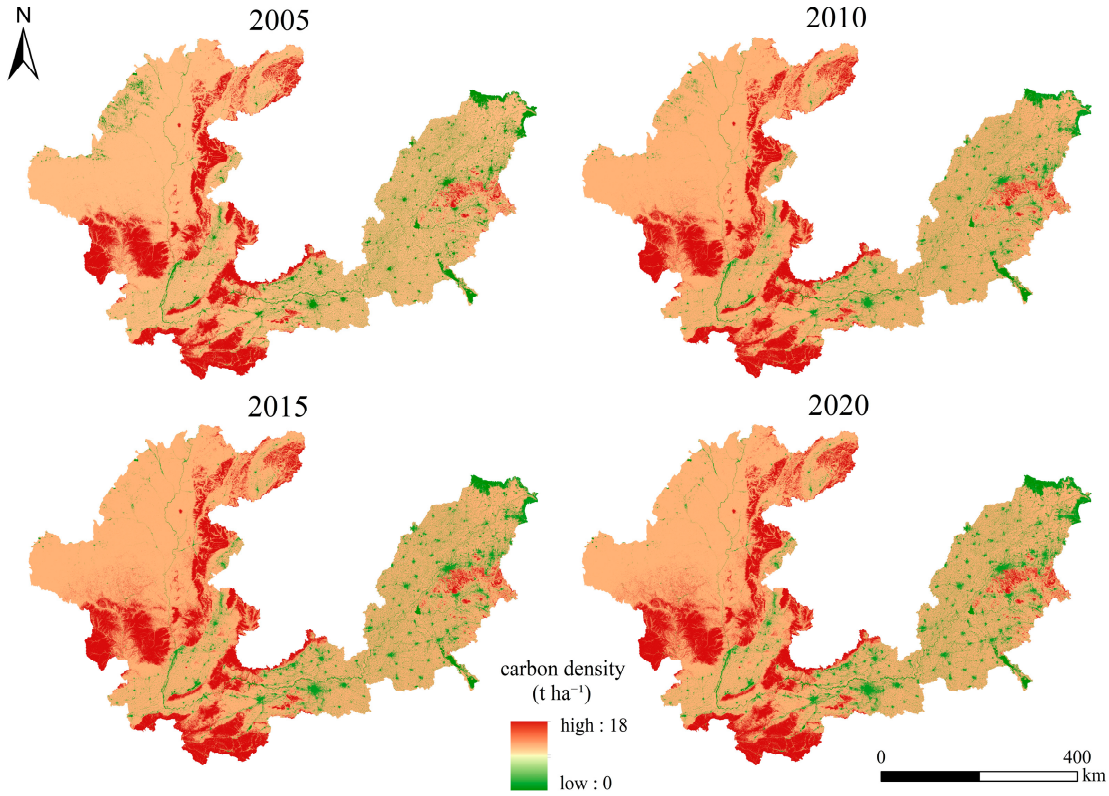

Figure 5. Spatial distribution of carbon density in the region along the MLYR from 2005 to 2020.

At the municipal scale, the carbon density values of 24 prefecture-level cities in the region along the MLYR ranged from 7 to 15 t ha^{-1} and exhibited a geographical distribution pattern that declined in magnitude from west to east. The only city with carbon density values lower than 9 t ha^{-1} was Dongying in Shandong province, mainly because it is situated in the mouth of the Yellow River, with a relatively large area of wetlands, mudflats, and other waters, and a high level of urban development that made its CL represent a relatively large proportion. The cities with carbon density values higher than 11 t ha^{-1} included Yulin, Yuncheng, Weinan, Jiyuan, Xinzhou, Linfen, Lvliang, Luoyang, Yan'an, and Sanmenxia in the region along the MYR because of the high proportion of WL. The carbon density values in other cities were in the range of 9 to 11 t ha^{-1}, mainly due to their location in the region along the LYR plain area with low vegetation cover and intense human disturbance (Table 5).

4.2.3. Spatial Clustering Characteristics of C-Storage

Hotspot analysis is a hidden-space clustering that identifies significant hotspots (high values) and cold spots (low values) within a given region by considering the distance between observed samples [44,45]. According to the size of the study area, this study conducted hotspot analysis at a specified distance of 5 km, determined the aggregation of C-storage, and identified the geographical distribution characteristics of hotspots and cold spots of C-storage.

Between 2005 and 2020, the arrangement of C-storage in the ecosystem within the area along the MLYR showed obvious clustering characteristics. The significant hotspot areas under 90% and 95% confidence levels were mostly distributed in the eastern, southern of the Loess Plateau, and southwestern Qinling Mountains and showed high-high aggregation characteristics, meaning that neighboring patches within high values of C-storage have a tendency to have similar values. The reasons are mainly due to the high altitude, undulating terrain, mainly FL, high vegetation coverage, and rich soil organic matter content (Figure 6). The cold spot area under confidence levels of 90%, 95%, and 99% was patchy, mainly in the form of clusters in the central-eastern North China Plain, and the C-storage showed the characteristics of low-low aggregation. The reason for this is that these regions were greatly influenced by human activities, with lower vegetation coverage, high land hardening or water, and low soil organic matter content.

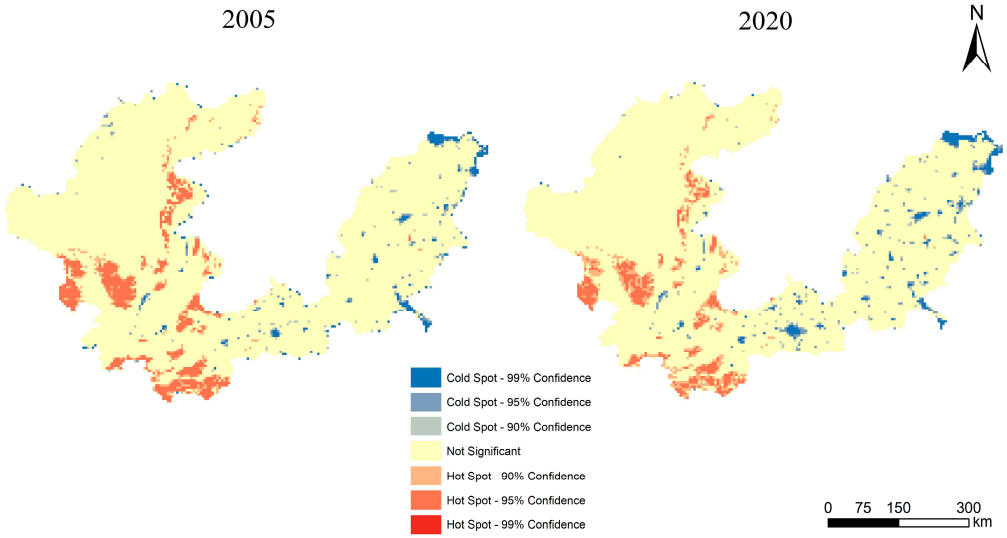

Figure 6. Hotspot distribution of C-storage in the region along the MLYR.

The spatial agglomerations of low-value C-storage in the area along the MLYR increased and those of high-value C-storage decreased from 2005 to 2020. The cold spot region demonstrated a gradual increment trend, and the percentage of cold-spot area under the 90%, 95%, and 99% confidence level increased by 0.86% from 12.10 × 10^5 ha to 14.75 × 10^5 ha. Overall,

a decreasing trend was observed in the hotspot area, from 28.70 × 10^5 ha to 26.05 × 10^5 ha. The hotspot area at 90% confidence level increased by 1.63% and the hotspot area at 95% confidence level decreased by 2.51%, but there was no hotspot area at 99% confidence level in both periods (Table 6).

Table 6. Cold spot and hotspot area statistics under different confidence levels.

Cold Hotspot Significance	2005		2020	
	Area (10^5 ha)	Proportion	Area (10^5 ha)	Proportion
Cold Spot—99% Confidence	5.25	1.73%	5.65	1.86%
Cold Spot—95% Confidence	3.30	1.09%	5.20	1.71%
Cold Spot—90% Confidence	3.55	1.17%	3.90	1.28%
Not Significant	262.98	86.57%	262.98	86.57%
Hotspot—90% Confidence	9.30	3.06%	14.25	4.69%
Hotspot—95% Confidence	19.40	6.39%	11.80	3.88%
Hotspot—99% Confidence	0	0	0	0

4.3. Analysis of the Drivers of Temporal and Spatial Changes in C-Storage

There are huge differences in terrain and climate between the region along the MYR and the LYR, which will inevitably lead to obvious difference in ecosystem C-storage. In order to obtain more accurate detection results, this study conducted factor detection for the region along the MYR and the LYR, respectively.

4.3.1. Dominant Factor Detection Analysis

In the region along the MYR, the spatial variation of ecosystem C-storage was mainly influenced by precipitation and temperature (we took the factors of $q > 0.5$ as predominant factors, factor of $0.3 < q < 0.5$ for the secondary factors), followed by FVC and elevation (Figure 7). It is worth mentioning that the impact of each component was decreased between 2005 and 2020 (Table 7). Precipitation and temperature could affect ecosystem C-storage by limiting vegetation productivity. Due to the predominant land utilization in the MYR area being FL and GL, which is rich in vegetation, meteorological factors had the most significant influence on C-storage in the area. FVC characterizes the degree of vegetation density and directly affects the accumulation of biological C-storage. The increase in elevation leads to a decrease in temperature that limits the proliferation of plants and the breakdown of organic carbon in the soil [6,46], especially in the loess plateau gully area; the difference in elevation will have a more significant effect on the spatial variation of C-storage.

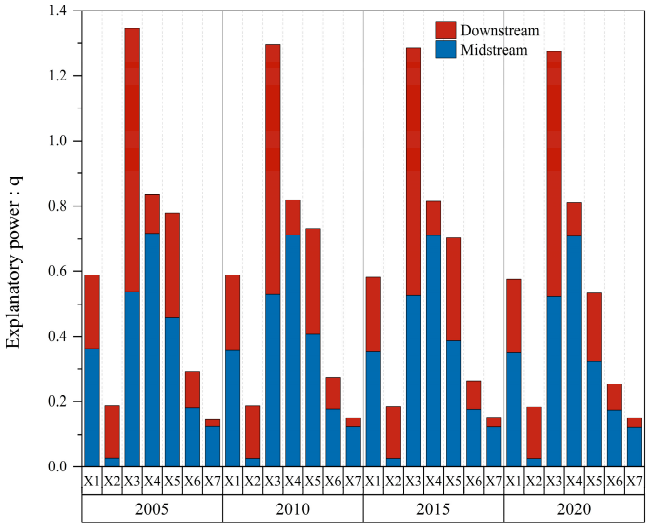

Figure 7. Comparison of q-value of factor detection of C-storage in the region along the MLYR in 2005, 2010, 2015, and 2020.

Table 7. The q-value of each factor in the region along the MYR.

	Elevation (X1)	Slope (X2)	Temperature (X3)	Precipitation (X4)	Fractional Vegetation Cover (X5)	Composite Land-Use Extent Index (X6)	Human Footprint (X7)
2005	0.3616	0.0283	0.5369	0.7168	0.4582	0.1805	0.1238
2010	0.3560	0.0279	0.5292	0.7127	0.4068	0.1772	0.1230
2015	0.3525	0.0276	0.5264	0.7112	0.3875	0.1764	0.1228
2020	0.3501	0.0274	0.5240	0.7092	0.3231	0.1747	0.1215
Total changes	−0.0115	−0.0010	−0.0129	−0.0076	−0.1350	−0.0058	−0.0023

In the region along the LYR, the spatial variation of ecosystem C-storage was mainly influenced by temperature, followed by FVC. Although the explanatory efficacy of most of the factors decreased, the explanatory power of human footprint, which characterizes human activity, increased (Figure 7 and Table 8). The primary cause is that the primary land-use type was arable dry land in the region along the LYR; crop development primarily hinges on appropriate temperature conditions. FVC directly affects net primary productivity (NPP) of vegetation, and NPP is the key to ecosystem C-storage. Something that deserves to be mentioned is that the human footprint is partly a reflection of the extent and intensity of the impact of human activities. Despite the lower explanatory power of the human footprint in this region compared to the region along the MYR, it increased by 0.0079 over the study period. Because of the rapid economic development in the region along the LYR, urban expansion caused by human activities had profoundly affected the land use pattern, which in turn affected C-storage. Moreover, elevation indirectly affected the distribution of C-storage by constraining the distribution of AL and FL.

Table 8. The q-value of each factor in the region along the LYR.

	Elevation (X1)	Slope (X2)	Temperature (X3)	Precipitation (X4)	Fractional Vegetation Cover (X5)	Composite Land-Use Extent Index (X6)	Human Footprint (X7)
2005	0.2273	0.1603	0.8086	0.1166	0.3204	0.1118	0.0203
2010	0.2329	0.1602	0.7670	0.1057	0.3250	0.0973	0.0267
2015	0.2301	0.1586	0.7589	0.1033	0.3159	0.0866	0.0284
2020	0.2274	0.1570	0.7508	0.1014	0.2102	0.0790	0.0282
Total changes	0.0001	−0.0034	−0.0578	−0.0152	−0.1103	−0.0328	0.0079

4.3.2. Interaction Factor Detection Analysis

The outcomes of the detection of interactions among the driving forces in different periods showed non-linear enhancement or two-factor enhancement, and there was no mutual independence or weakening. This signifies that the explanatory strength of the interaction among the factors on the spatial distribution changes of C-storage was increased to different extents in comparison to the impact of a single factor. Thus, the spatial arrangement of C-storage undergoes alterations is a complex process of factor interaction that was confirmed.

In the region along the MYR, the interaction between slope and elevation, CLEI, and human footprint showed non-linearly enhanced in 2005–2015. In 2020, the interaction between FVC and CLEI also showed non-linearly enhanced. For the interaction of all other factors, there was two-factor enhancement in four different time periods, and the interaction of precipitation and temperature exhibited the strongest explanatory capacity for the variation in C-storage across the space-time variation (Figure 8). The effects of the correlation between precipitation and other variables on the space-time variation of C-storage all exceeded 0.7, and the effects of the interaction between temperature and other factors on the space-time variation of C-storage all exceeded 0.5.

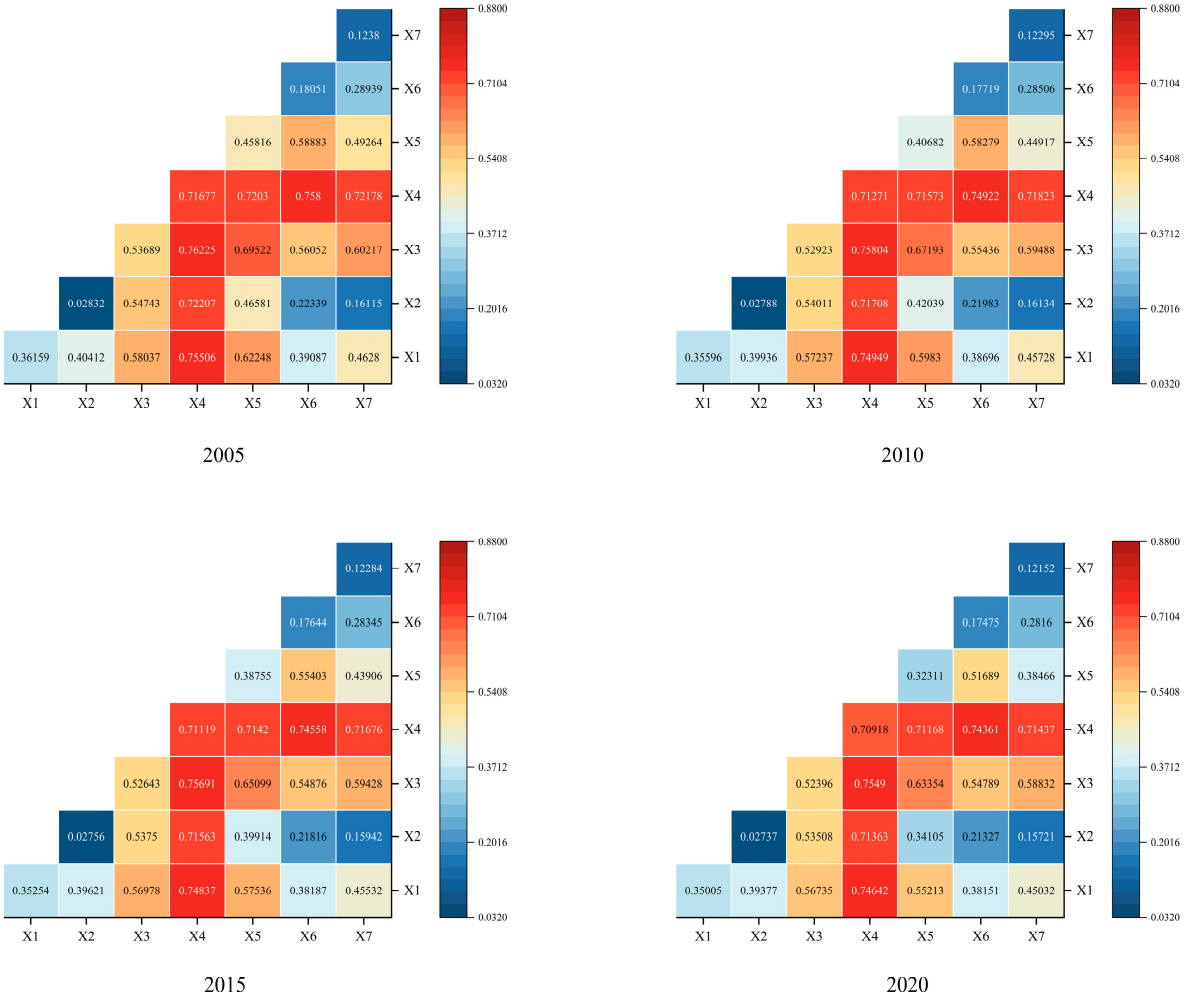

Figure 8. Heatmap of q-value of C-storage interaction factor detection in the region along the MYR in 2005, 2010, 2015, and 2020.

In the region along the LYR, the interaction between precipitation and elevation, slope, FVC, CLEI, and human footprint showed non-linearly enhanced in four different periods, as did between human footprint and elevation, slope, and CLEI. For the interaction of all other factors, there was a two-factor enhancement in four different time periods. The interaction between precipitation and temperature had the strongest explanatory power for the space-time variation of C-storage (Figure 9). As well as the interaction effects between temperature and other factors on the space-time variation of C-storage, all exceeded 0.7. The dominant factor in this region was temperature, and the q-values indicating the interaction between temperature and the various other elements reached their peak values in each period.

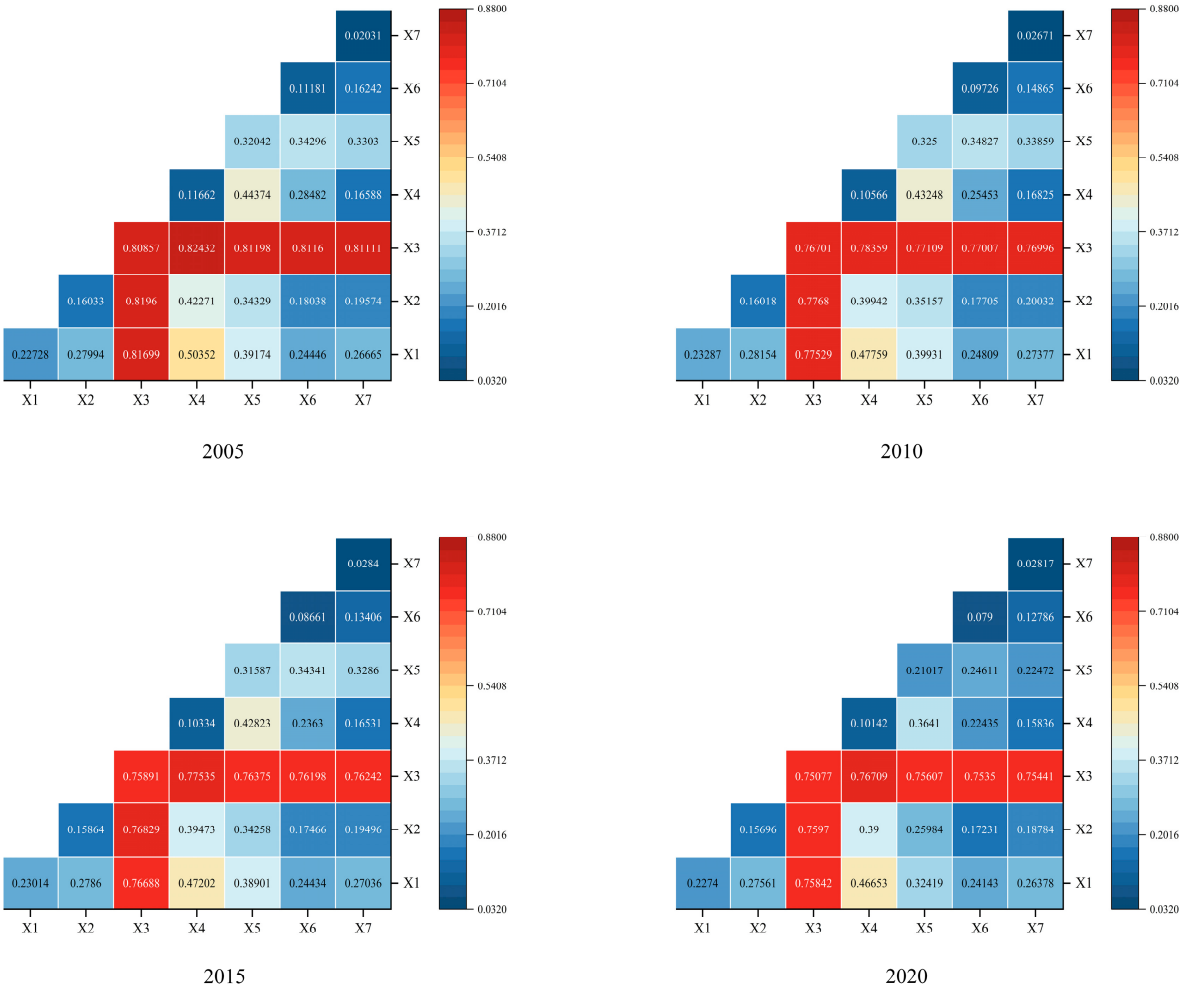

Figure 9. Heatmap of q-value of C-storage interaction factor detection in the region along the LYR in 2005, 2010, 2015, and 2020.

5. Discussion

This study used the InVEST model and GeoDetector to systematically analyze the spatiotemporal evolution of C-storage and its influencing factors in the region along the MLYR. By comparing results from similar regions, the accuracy of this study's findings was validated to some extent. Duan et al. [47] explored ecosystem C-storage before and after the Grain for Green Project in the Yellow River Basin, concluding that carbon density in Yulin, Xinzhou, Linfen, and Yan'an increased from 2000 to 2020. Despite differing study periods, these findings coincide with our conclusions. A comparison reveals that the C-storage distribution in the region along the MYR in 2020, as found in this study, is consistent with Xu et al.'s [27] spatial distribution for the corresponding area. Li et al. [48] highlighted the significant influence of elevation and precipitation on C-storage in the Loess Plateau. Similarly, our study identified precipitation as the dominant factor in the region along the MYR, with elevation also being a critical factor. Additionally, our study revealed the dynamic impact of human activity on C-storage over long-term scales, providing a more comprehensive analysis of influencing factors. In the analysis of C-storage aggregation characteristics, we found a significant increase in low-value C-storage aggregation in the Yellow River Delta, consistent with Ma et al.'s [28] findings on coastal blue carbon in the Yellow River Delta. Nonetheless, carbon density has always been the key to accurately assessing C-storage [49]. Measured data is an essential source for the evaluation of C-storage and their changes, and although the carbon-intensity data in the present study have been corrected for climate data, their accuracy is still difficult to compare with measured values.

Therefore, in future research, we will adopt the way of quadrat measurement to obtain the carbon density values of different land types and soil types and correct them to increase the precision of C-storage output results.

To identify the causative factors influencing C-storage in the region along the MLYR, the whole study area was initially selected. However, only a subset of the factors demonstrated an explanatory power that exceeded 0.1. Furthermore, the driver analysis revealed that the *p*-values of certain factors were not statistically significant. Through the analysis of the research results, we believed that the results do not precisely reflect the influence of each factor on the spatial arrangement of C-storage. Therefore, we considered that the main reason the results were less than satisfactory was that the natural environment, human activities, and ecological characteristics of the region along the MYR and LYR were vastly different and had few commonalities, resulting in large inaccuracies in the detection of factors across the study area. Therefore, the whole study area was split into two sections, the region along the MYR and the region along the LYR, for which the space-time variation drivers of C-storage were analyzed separately, and the zonal detection can greatly improve the research accuracy.

This paper identified and analyzed the cold spot and hotspot areas of C-storage, and the results indicated that the aggregation effect of low values of C-storage strengthened and the aggregation effect of high values of C-storage weakened. Therefore, we should adopt relevant protection measures for the hotspot areas of C-storage, such as returning farmland to forests or grasses, and strictly adhering to the "red line" of forestry. In the cold spot area of C-storage, the predicted area should be protected as far as possible, the development of CL should be carried out in accordance with national land space planning to avoid blindness as far as possible, and development should be combined with protection in the process of regional construction. As for the increase in the cold spot area in the eastern region, especially at the Yellow River Estuary, we considered that the increase in the area of water which is about the primary cause is the establishment of wetland protection policies. In addition, the Yellow River Delta in China exhibits the highest level of dynamic changes between land and sea among all deltas in the world. The coastline of the Yellow River Delta from 1976 to 2020 demonstrated a spatial configuration of retreat to land in the north and expansion to sea in the south. Overall, the Yellow River Delta is currently experiencing a phase of decline since 1990 [50,51], which implied that the waters in this study area tended to increase during the study time period, leading to the intensification of the agglomeration effect of low C-storage.

6. Conclusions

Based on LUCC data, C-storage in the region along the MLYR from 2005 to 2020 was measured and patterns of spatiotemporal variation in C-storage were analyzed. Then, we were able to detect key drivers of spatiotemporal variation in C-storage and their interactions. The primary research findings are listed below:

(1) Between 2005 and 2020, there was a consistent reduction in the expanse of AL, with CL, FL, and UL all exhibiting a rising trend and the area of GL and WL being basically stable in the region along the MLYR. The largest increase of CL mainly transferred from AL; The area of AL decreased the most and was mostly attributed to its transformation into GL and CL.

(2) During the period of 2005–2020, the C-storage exhibited a continuous reduction trend. The total C-storage decreased at a rate of 1% in 2015–2020, which was the phase with the largest change in C-storage. The C-storage in the region along the MLYR exhibited a consistent geographical distribution pattern, characterized by high values in the western region and low values in the eastern region. With the development of time, the agglomeration effect of low-value C-storage strengthened and the aggregation effect of high-value C-storage weakened.

(3) From 2005 to 2020, meteorological factors were the dominant factors influencing the spatiotemporal variation of C-storage in the region along the MYR, with ele-

vation and FVC as secondary factors; slope had the least explanatory power. The primary determinant affecting the spatiotemporal variation of C-storage along the LYR was temperature, with FVC as a secondary factor; human footprint had the least explanatory power.

(4) The results of interaction detection among drivers in all four periods showed nonlinear enhancement or double-factor enhancement. We discovered that the correlation between temperature and precipitation exhibited the highest degree, and both factors had the greatest ability to explain the spatiotemporal variation of C-storage within both the MYR and LYR regions.

C-storage and carbon emission are crucial components of ecological balance, which is fundamental to sustainable development. Investigating C-storage in the region along the MLYR not only enhances our understanding of regional land resource utilization, but also aids in the formulation of policies for promoting sustainability in the area. By elucidating the connections between C-storage dynamics, human activities, and sustainable land management, this study provided scientific evidence for policymakers to develop strategies that balance economic development with environmental conservation, ensuring long-term sustainability in the region. Moving forward, efforts will be made to refine measurement methodologies related to C-storage and to promote the formulation of regional sustainability development plans based on more precise data.

Author Contributions: Conceptualization, S.A. and Y.D.; methodology, S.A. and Y.D.; software, S.A.; validation, S.A., Y.D., D.C. and X.W.; formal analysis, S.A. and Y.D.; investigation, S.A. and X.W.; resources, S.A.; data curation, S.A.; writing—original draft preparation, S.A.; writing—review and editing, S.A. and Y.D.; visualization, S.A.; supervision, Y.D. and D.C.; project administration, Y.D.; funding acquisition, Y.D. All authors have read and agreed to the published version of the manuscript.

Funding: This research was funded by the Natural Science Foundation of Shandong Province, China, grant number NO. ZR2021MD110, and the Doctoral Foundation of Liaocheng University, grant number NO. 318052117.

Institutional Review Board Statement: Not applicable.

Informed Consent Statement: Not applicable.

Data Availability Statement: Data is available upon request.

Conflicts of Interest: The authors declare no conflicts of interest.

References

1. Liu, Q.; Zhang, W.; Yao, M.; Yuan, J. Carbon emissions performance regulation for China's top generation groups by 2020: Too challenging to realize? *Resour. Conserv. Recycl.* **2017**, *122*, 326–334. [CrossRef]
2. Dong, F.; Yu, B.; Hadachin, T.; Dai, Y.; Wang, Y.; Zhang, S.; Long, R. Drivers of carbon emission intensity change in China. *Resour. Conserv. Recycl.* **2018**, *129*, 187–201. [CrossRef]
3. Fernando, Y.; Hor, W.L. Impacts of energy management practices on energy efficiency and carbon emissions reduction: A survey of malaysian manufacturing firms. *Resour. Conserv. Recycl.* **2017**, *126*, 62–73. [CrossRef]
4. Makkonen, M.; Huttunen, S.; Primmer, E.; Repo, A.; Hildén, M. Policy coherence in climate change mitigation: An ecosystem service approach to forests as carbon sinks and bioenergy sources. *For. Policy Econ.* **2015**, *50*, 153–162. [CrossRef]
5. Xi, F.; Lin, G.; Zhao, Y.; Li, X.; Chen, Z.; Cao, C. Land Use Optimization and Carbon Storage Estimation in the Yellow River Basin, China. *Sustainability* **2023**, *15*, 11278. [CrossRef]
6. Wang, X.; Wu, J.; Liu, Y.; Hai, X.; Shanguan, Z.; Deng, L. Driving factors of ecosystem services and their spatiotemporal change assessment based on land use types in the Loess Plateau. *J. Environ. Manag.* **2022**, *311*, 114835. [CrossRef] [PubMed]
7. Barakat, A.; Ouargaf, Z.; Touhami, F. Identification of potential areas hosting aggregate resources using GIS method: A case study of Tadla-Azilal Region, Morocco. *Environ. Earth Sci.* **2016**, *75*, 774. [CrossRef]
8. Zang, S.Y.; Huang, X.; Na, X.D.; Sun, L. An assessment approach of land-use to resource-based cities: A case study on land-use process of Daqing region. *Int. J. Environ. Sci. Technol.* **2015**, *12*, 3827–3836. [CrossRef]
9. Yang, F.; Zeng, G.; Du, C.; Tang, L.; Zhou, J.; Li, Z. Spatial analyzing system for urban land-use management based on GIS and multi-criteria assessment modeling. *Prog. Nat. Sci.* **2008**, *18*, 1279–1284. [CrossRef]

10. Meyer, M.A.; Früh-Müller, A. Patterns and drivers of recent agricultural land-use change in Southern Germany. *Land Use Policy* **2020**, *99*, 104959. [CrossRef]
11. Tang, L.; Ke, X.; Zhou, T.; Zheng, W.; Wang, L. Impacts of cropland expansion on carbon storage: A case study in Hubei, China. *J. Environ. Manag.* **2020**, *265*, 110515. [CrossRef]
12. Liu, Q.; Yang, D.; Cao, L.; Anderson, B. Assessment and Prediction of Carbon Storage Based on Land Use/Land Cover Dynamics in the Tropics: A Case Study of Hainan Island, China. *Land* **2022**, *11*, 244. [CrossRef]
13. Urgilez-Clavijo, A.; Rivas-Tabares, D.; Gobin, A.; de la Riva, J. Comprehensive Framework for Analysing the Intensity of Land Use and Land Cover Change in Continental Ecuadorian Biosphere Reserves. *Sustainability* **2024**, *16*, 1566. [CrossRef]
14. Holdaway, R.J.; McNeill, S.J.; Mason, N.W.; Carswell, F.E. Propagating uncertainty in plot-based estimates of forest carbon stock and carbon stock change. *Ecosystems* **2014**, *17*, 627–640. [CrossRef]
15. Izaurralde, R.C.; Rice, C.W.; Wielopolski, L.; Ebinger, M.H.; Reeves, J.B., III; Thomson, A.M.; Harris, R.; Francis, B.; Mitra, S.; Rappaport, A.G.; et al. Evaluation of Three Field-Based Methods for Quantifying Soil Carbon. *PLoS ONE* **2013**, *8*, e55560. [CrossRef] [PubMed]
16. Zhao, J.; Xie, H.; Ma, J.; Wang, K. Integrated remote sensing and model approach for impact assessment of future climate change on the carbon budget of global forest ecosystems. *Glob. Planet. Chang.* **2021**, *203*, 103542. [CrossRef]
17. Singh, P.; Benbi, D.K. Modeling Soil Organic Carbon with DNDC and RothC Models in Different Wheat-Based Cropping Systems in North-Western India. *Commun. Soil Sci. Plant Anal.* **2020**, *51*, 1184–1203. [CrossRef]
18. Mao, F.; Du, H.; Zhou, G.; Li, X.; Xu, X.; Li, P.; Sun, S. Coupled LAI assimilation and BEPS model for analyzing the spatiotemporal pattern and heterogeneity of carbon fluxes of the bamboo forest in Zhejiang Province, China. *Agric. For. Meteorol.* **2017**, *242*, 96–108. [CrossRef]
19. Liu, K.; Zhang, C.; Zhang, H.; Xu, H.; Xia, W. Spatiotemporal Variation and Dynamic Simulation of Ecosystem Carbon Storage in the Loess Plateau Based on PLUS and InVEST Models. *Land* **2023**, *12*, 1065. [CrossRef]
20. Xie, L.; Bai, Z.; Yang, B.; Fu, S. Simulation Analysis of Land-Use Pattern Evolution and Valuation of Terrestrial Ecosystem Carbon Storage of Changzhi City, China. *Land* **2022**, *11*, 1270. [CrossRef]
21. Li, K.; Cao, J.; Adamowski, J.F.; Biswas, A.; Zhou, J.; Liu, Y.; Zhang, Y.; Liu, C.; Dong, X.; Qin, Y. Assessing the effects of ecological engineering on spatiotemporal dynamics of carbon storage from 2000 to 2016 in the Loess Plateau area using the InVEST model: A case study in Huining County, China. *Environ. Dev.* **2021**, *39*, 100641. [CrossRef]
22. Wu, F.; Wang, Z. Assessing the impact of urban land expansion on ecosystem carbon storage: A case study of the Changzhutan metropolitan area, China. *Ecol. Indic.* **2023**, *154*, 110688. [CrossRef]
23. Ye, S.; Laws, E.A.; Yuknis, N.; Ding, X.; Yuan, H.; Zhao, G.; Wang, J.; Yu, X.; Pei, S.; DeLaune, R.D. Carbon Sequestration and Soil Accretion in Coastal Wetland Communities of the Yellow River Delta and Liaohe Delta, China. *Estuaries Coasts* **2015**, *38*, 1885–1897. [CrossRef]
24. Zhu, L.; Song, R.; Sun, S.; Li, Y.; Hu, K. Land use/land cover change and its impact on ecosystem carbon storage in coastal areas of China from 1980 to 2050. *Ecol. Indic.* **2022**, *142*, 109178. [CrossRef]
25. Liang, Y.; Hashimoto, S.; Liu, L. Integrated assessment of land-use/land-cover dynamics on carbon storage services in the Loess Plateau of China from 1995 to 2050. *Ecol. Indic.* **2021**, *120*, 106939. [CrossRef]
26. Myeong, S.; Nowak, D.J.; Duggin, M.J. A temporal analysis of urban forest carbon storage using remote sensing. *Remote Sens. Environ.* **2006**, *101*, 277–282. [CrossRef]
27. Xu, C.; Zhang, Q.; Yu, Q.; Wang, J.; Wang, F.; Qiu, S.; Ai, M.; Zhao, J. Effects of land use/cover change on carbon storage between 2000 and 2040 in the Yellow River Basin, China. *Ecol. Indic.* **2023**, *151*, 110345. [CrossRef]
28. Ma, T.; Li, X.; Bai, J.; Ding, S.; Zhou, F.; Cui, B. Four decades' dynamics of coastal blue carbon storage driven by land use/land cover transformation under natural and anthropogenic processes in the Yellow River Delta, China. *Sci. Total Environ.* **2019**, *655*, 741–750. [CrossRef]
29. Yang, J.; Huang, X. The 30 m Annual Land Cover Datasets and Its Dynamics in China from 1985 to 2022. 2023. Available online: https://zenodo.org/records/8176941 (accessed on 1 January 2023).
30. Liu, J.; Liu, M.; Tian, H.; Zhuang, D.; Zhang, Z.; Zhang, W.; Tang, X.; Deng, X. Spatial and temporal patterns of China's cropland during 1990–2000: An analysis based on Landsat TM data. *Remote Sens. Environ.* **2005**, *98*, 442–456. [CrossRef]
31. Zhuang, D.; Liu, J. Study on the model of regional differentiation of land use degree in China. *J. Nat. Resour.* **1997**, *12*, 105–111. [CrossRef]
32. Peng, S. *1-km Monthly Mean Temperature Dataset for China (1901–2022)*; National Tibetan Plateau Data Center: Beijing, China, 2020. [CrossRef]
33. Peng, S. *1-km Monthly Precipitation Dataset for China (1901–2022)*; National Tibetan Plateau Data Center: Beijing, China, 2020. [CrossRef]
34. Gao, J.; Zhang, H.; Zhang, W.; Chen, X.; Shen, W.; Xiao, T.; Zhang, Y.; Shi, Y. *China Regional 250m Fractional Vegetation Cover Data Set (2000–2023)*; National Tibetan Plateau Data Center: Beijing, China, 2024. [CrossRef]
35. Mu, H.; Li, X.; Wen, Y.; Huang, J.; Du, P.; Su, W.; Miao, S.; Geng, M. A global record of annual terrestrial Human Footprint dataset from 2000 to 2018. *Sci. Data* **2022**, *9*, 176. [CrossRef]
36. Yang, J.; Xie, B.; Zhang, D. Spatial and temporal variation of carbon stocks in the Yellow River basin based on InVEST and CA-Markov models. *Chin. J. Ecol. Agric.* **2021**, *29*, 1018–1029. [CrossRef]

37. Alam, S.A.; Starr, M.; Clark, B.J.F. Tree biomass and soil organic carbon densities across the Sudanese woodland savannah: A regional carbon sequestration study. *J. Arid Environ.* **2013**, *89*, 67–76. [CrossRef]
38. Giardina, C.P.; Ryan, M.G. Evidence that decomposition rates of organic carbon in mineral soil do not vary with temperature. *Nature* **2000**, *404*, 858–861. [CrossRef]
39. Chen, G.; Yang, Y.; Liu, L.; Li, X.; Zhao, Y.; Yuan, Y. Progress of forest subsurface carbon allocation (TBCA) research. *J. Subtrop. Resour. Environ.* **2007**, *2*, 34–42. [CrossRef]
40. Su, Y.; Li, T.; Cheng, S.; Wang, X. Spatial distribution exploration and driving factor identification for soil salinisation based on geodetector models in coastal area. *Ecol. Eng.* **2020**, *156*, 105961. [CrossRef]
41. Zhao, Y.; Liu, L.; Kang, S.; Ao, Y.; Han, L.; Ma, C. Quantitative Analysis of Factors Influencing Spatial Distribution of Soil Erosion Based on Geo-Detector Model under Diverse Geomorphological Types. *Land* **2021**, *10*, 604. [CrossRef]
42. Wang, J.; Xu, C. Geodetector: Principle and prospective. *Acta Geogr. Sin.* **2017**, *72*, 116–134. [CrossRef]
43. Wang, J.; Li, X.; Christakos, G.; Liao, Y.; Zhang, T.; Gu, X.; Zheng, X. Geographical Detectors-Based Health Risk Assessment and its Application in the Neural Tube Defects Study of the Heshun Region, China. *Int. J. Geogr. Inf. Sci.* **2010**, *24*, 107–127. [CrossRef]
44. He, Y.; Ma, J.; Zhang, C.; Yang, H. Spatio-Temporal Evolution and Prediction of Carbon Storage in Guilin Based on FLUS and InVEST Models. *Remote Sens.* **2023**, *15*, 1445. [CrossRef]
45. Zhao, M.; He, Z.; Du, J.; Chen, L.; Lin, P.; Fang, S. Assessing the effects of ecological engineering on carbon storage by linking the CA-Markov and InVEST models. *Ecol. Indic.* **2019**, *98*, 29–38. [CrossRef]
46. Wang, Z.; Li, X.; Mao, Y.-t.; Li, L.; Wang, X.; Lin, Q. Dynamic simulation of land use change and assessment of carbon storage based on climate change scenarios at the city level: A case study of Bortala, China. *Ecol. Indic.* **2022**, *134*, 108499. [CrossRef]
47. Duan, X.; Han, M.; Kong, X.; Sun, J.; Zhang, H. Spatiotemporal evolution and simulation prediction of ecosystem carbon storage in the Yellow River Basin before and after the Grain for Green Project. *Environ. Sci.* **2024**, 1–18. Available online: https://link.cnki.net/urlid/11.1895.x.20240221.1159.007 (accessed on 1 July 2024).
48. Li, M.; Shangguan, Z.; Deng, L. Spatial distribution of carbon storage in the terrestrial ecosystems and its influencing factors on the Loess Plateau. *Acta Ecol. Sin.* **2021**, *41*, 6786–6799. [CrossRef]
49. Deng, Y.; Jiang, W.; Wu, Z.; Peng, K.; Ling, Z.; Li, Z.; Wang, X. Assessing and Characterizing Carbon Storage in Wetlands of the Guangdong–Hong Kong–Macau Greater Bay Area, China, During 1995–2020. *IEEE J. Sel. Top. Appl. Earth Obs. Remote Sens.* **2022**, *15*, 6110–6120. [CrossRef]
50. Zhu, Q.; Li, P.; Li, Z.; Pu, S.; Wu, X.; Bi, N.; Wang, H. Spatiotemporal Changes of Coastline over the Yellow River Delta in the Previous 40 Years with Optical and SAR Remote Sensing. *Remote Sens.* **2021**, *13*, 1940. [CrossRef]
51. Li, C.; Zhu, L.; Dai, Z.; Wu, Z. Study on Spatiotemporal Evolution of the Yellow River Delta Coastline from 1976 to 2020. *Remote Sens.* **2021**, *13*, 4789. [CrossRef]